Research Square

Preprints are preliminary reports that have not undergone peer review.
They should not be considered conclusive, used to inform clinical practice,
or referenced by the media as validated information.

Multidecadal variability of the ENSO early-winter teleconnection to the North Atlantic in CMIP6 models: robustness and mechanisms

Pablo Fernández-Castillo

pablof16@ucm.es

Instituto de Geociencias https://orcid.org/0000-0003-3441-2030

Belén Rodríguez-Fonseca

Complutense University of Madrid https://orcid.org/0000-0002-5261-7083

Teresa Losada

Complutense University of Madrid https://orcid.org/0000-0002-8430-1745

Christopher O'Reilly

University of Reading https://orcid.org/0000-0002-8630-1650

Muhammad Adnan Abid

University of Oxford https://orcid.org/0000-0002-7389-7977

Research Article

Keywords: ENSO, teleconnection, NAO, early, winter, seasonal, North Atlantic, Europe, variability, EAP, early-winter, CMIP

Posted Date: July 23rd, 2026

DOI: https://doi.org/10.21203/rs.3.rs-10430443/v1

License: This work is licensed under a Creative Commons Attribution 4.0 International License.
Read Full License

Additional Declarations: The authors declare no competing interests.

ORIGINAL ARTICLE

Journal Section

Multidecadal variability of the ENSO early-winter teleconnection to the North Atlantic in CMIP6 models: robustness and mechanisms

Pablo Fernández-Castillo[1,2,3] | **Belén Rodríguez-Fonseca**[2,1] | **Teresa Losada**[2] | **Christopher O'Reilly**[3] | **Muhammad Adnan Abid**[4,5]

[1]Instituto de Geociencias (IGEO), CSIC-UCM, Madrid, Spain

[2]Departamento de Física de la Tierra y Astrofísica, Universidad Complutense de Madrid, Madrid, Spain

[3]Department of Meteorology, University of Reading, Reading, United Kingdom

[4]Atmospheric, Oceanic and Planetary Physics (AOPP), Department of Physics, University of Oxford, Oxford, United Kingdom

[5]National Centre for Atmospheric Science (NCAS), United Kingdom

Correspondence
Pablo Fernández-Castillo, Instituto de Geociencias (IGEO), CSIC-UCM, Madrid, Spain
Email: pablof16@ucm.es

Funding information

Observational studies have found that the El Niño-Southern Oscillation (ENSO) significantly affects the North Atlantic atmospheric circulation in the early winter season (November-December), favouring seasonal-mean circulation anomalies that project onto the East Atlantic Pattern (EAP). Recent analyses have found that this teleconnection has changed across different epochs, which has relevant implications for seasonal predictability in the North Atlantic and Europe. However, these analyses were solely based on observations, and the limited length of the instrumental period poses a heavy constraint on a robust assessment of whether this multidecadal variability is indeed significant and what its underlying dynamical mechanisms are. In this study, we address these two important questions by using long pre-industrial control simulations, which allow us to overcome the constraints related to small sample sizes in the observations. Our results show a significant chance that the multidecadal variability of the ENSO-EAP teleconnection is not explained just by sampling variability, but is likely driven by dynami-

[*] Equally contributing authors.

cal mechanisms. While the analysis of individual models reveals a high degree of uncertainty in the teleconnection and the mechanisms driving its multidecadal variability, changes in the tropical Indian Ocean convection, PDO phase and background state of the jet stream emerge as potential mechanisms explaining the non-stationarity of the teleconnection. These results enhance our understanding of seasonal variability and predictability in the North Atlantic and Europe.

KEYWORDS
ENSO, teleconnection, Europe, stationarity , variability, multidecadal

1 | INTRODUCTION

The El Niño-Southern Oscillation (ENSO) is the leading mode of global climate variability at interannual timescales. Despite taking place over the equatorial Pacific, the impacts of ENSO can extend to many regions worldwide by means of its teleconnections (Ropelewski and Halpert, 1987; Kiladis and Diaz, 1989), including the North Atlantic and Europe (Brönnimann, 2007). The influence of ENSO over this area is not particularly strong and is frequently overwhelmed by the large internal variability characteristic of this region, which makes it difficult to isolate the forced signal (Brands, 2017; Deser et al., 2018). Nevertheless, the ENSO forcing on the North Atlantic circulation provides a potentially predictable signal at seasonal timescales; thus, a comprehensive understanding of ENSO and its teleconnections is key to assessing seasonal predictability in this region.

The impacts of ENSO on the North Atlantic and European region depend on the season (Mariotti et al., 2002; Brönnimann, 2007) and can be sensitive to the magnitude and/or spatial configuration of the sea surface temperature (SST) anomalies over the tropical Pacific (Toniazzo and Scaife, 2006; Graf and Zanchettin, 2012; Hardiman et al., 2019; McKenna and Karamperidou, 2023). Furthermore, even within the same season, these impacts can depend on the period analysed (Rodríguez-Fonseca et al., 2016). In particular, in the early winter season (November-December) ENSO has been found to primarily influence the East Atlantic Pattern (EAP), which represents the second leading mode of atmospheric circulation variability in the North Atlantic (Ayarzagüena et al., 2018; King et al., 2018; O'Reilly et al., 2024). In its positive phase, the EAP is characterised by a centre of negative mean sea-level pressure anomalies west of the British Isles, bringing wetter- and milder-than-average conditions to western Europe, while anomalies of the opposite sign are favoured under the negative phase of the EAP. Operational seasonal forecasting systems based on dynamical models generally capture the spatial pattern of the ENSO-EAP teleconnection reasonably well and, despite an underestimation of the magnitude of the resulting circulation anomalies over the North Atlantic, they exhibit moderate forecast skill in this region (Molteni and Brookshaw, 2023; Raganato et al., 2025; O'Reilly, 2025; Fernández-Castillo et al., 2025).

ENSO can influence the North Atlantic circulation through tropospheric and stratospheric pathways. In early winter,

when stratospheric coupling remains weak, the tropospheric pathway dominates (Ayarzagüena et al., 2018; O'Reilly et al., 2024). Specifically, ENSO-related tropical convection anomalies in different tropical regions lead to anomalies in the divergent wind in the upper levels of the troposphere. When the poleward component of these divergent wind anomalies interacts with the meridional gradient of planetary vorticity, it can act as a source of Rossby waves (Sardeshmukh and Hoskins, 1988). Under a favourable configuration of the jet stream, these waves may propagate polewards (Hoskins and Karoly, 1981). While this direct Rossby wave response is mainly confined to the tropics and the subtropics, the feedback between synoptic eddies and the mean flow can further strengthen the mean flow anomalies and play a crucial role in shaping up the seasonal mean response to ENSO in the midlatitudes (Harnik et al., 2010; Li and Lau, 2012; Jiménez-Esteve and Domeisen, 2018). For the early-winter season specifically, the main regions of tropical convection anomalies that can contribute to this teleconnection include the eastern tropical Pacific, the Indian Ocean (Abid et al., 2021, 2023), and the Gulf of Mexico–Caribbean Sea (Ayarzagüena et al., 2018). In this way, El Niño events are characterised by a zonal extension of the North Pacific jet and storm track, favouring a more southward position of the jet stream in the midlatitudes of the North Atlantic and seasonal-mean circulation anomalies that project onto a positive EAP. Conversely, the La Niña events generally feature a more disjointed North Pacific-North Atlantic jet structure, which favours more frequent poleward jet excursions in the North Atlantic (O'Reilly et al., 2024) and contribute to seasonal-mean circulation anomalies that project onto a negative EAP.

Importantly, ENSO teleconnections can exhibit non-stationarity, meaning that the teleconnection may change across different epochs (Rodríguez-Fonseca et al., 2016). Given the role of the tropical wave sources and the propagation of these waves in the teleconnection, a change in any of these can potentially lead to a different response of the jet stream and storm track over the North Pacific. The feedback from synoptic eddies may contribute to further amplify these differences over the North Atlantic, shaping up a substantially different teleconnection pattern there. Nevertheless, the stationarity of the early-winter teleconnection to the North Atlantic is only starting to be addressed. Most of the literature on the early winter teleconnection supported an ENSO-EAP teleconnection, but these studies employed a stationary framework, i.e. the teleconnection was analysed using the whole available period, assuming stationarity. However, by partitioning the observational record into different subperiods, recent studies have found that this teleconnection exhibits substantial multidecadal variability. In particular, from the late 1970s to the late 1990s, ENSO was mainly correlated with the NAO rather than the EAP, while from the late 1990s onwards the link to the EAP has strengthened at the expense of the NAO (Hou et al., 2023; Fernández-Castillo et al., 2025). Furthermore, there are indications that the ENSO-EAP link was very weak in the first half of the 20th century. These changes in the teleconnection have resulted in substantially different seasonal predictability patterns of surface climate in Europe, which brings up the need to understand why changes in the early winter teleconnection are occurring. (Fernández-Castillo et al., 2025).

Still, much remains to be understood about the multidecadal variability of the ENSO early-winter teleconnection to the North Atlantic. In particular, while the two studies addressing the stationarity of this teleconnection provided relevant insights, they relied solely on observational and reanalysis data, which poses certain limitations. Assessing non-stationarity inherently requires partitioning the analysis period into distinct multidecadal sub-periods and analysing the teleconnection in each of them. However, the relatively short instrumental record notably restricts the sample size within these epochs, thereby limiting the statistical robustness of the detected changes. These limitations become even bigger when trying to relate changes in the teleconnection to low-frequency modes of variability of the climate system, such as the Pacific Decadal Oscillation (PDO) or the Atlantic Multidecadal Variability (AMV), as barely a full cycle or two lie within the instrumental record. For instance, in the last few decades, the link between ENSO and the EAP has been observed stronger in the negative PDO phase, while the period with a weaker link to the

EAP coincided with the positive phase of the PDO (Fernández-Castillo et al., 2025), but to what extent this may have been coincidental or is suggestive of a possible modulating effect is a question that cannot be addressed just with observational data. Understanding the possible role of low-frequency variability on the teleconnection is of crucial importance and has relevant implications for seasonal variability and predictability.

In this study, we analyse the ENSO early-winter teleconnection to the North Atlantic in a set of pre-industrial control (piControl) simulations of models participating in the latest Coupled Model Intercomparison Project (CMIP6). The main objective is to evaluate whether there is a significant multidecadal variability involved in this teleconnection within the models and, in such case, what mechanisms are potentially driving it. By using long model integrations, we overcome the sample size constraints inherent to the observational record, thus providing a more robust framework to answer our motivating questions. Our analyses reveal a significant chance that the multidecadal variability of the ENSO-EAP teleconnection in early winter cannot be explained just by sampling variability, but is likely driven to some extent by dynamical mechanisms. Changes in the tropical convection over the Indian Ocean and multidecadal changes in the mean state of the jet stream and in the PDO state emerge as the most plausible mechanisms explaining this multidecadal variability.

2 | DATA AND METHODS

2.1 | Data

Data from piControl simulations of models participating in the Coupled Model Intercomparison Project phase 6 (CMIP6) (Eyring et al., 2016) are used in this study. In these simulations, anthropogenic forcings are fixed at 1850 levels, while time-averaged natural forcings are prescribed. The long simulation period (spanning several centuries) and the constant forcing conditions provide an adequate framework to assess the stationarity of the teleconnection and its possible modulation from low-frequency natural variability, including modes such as the PDO or AMV. In order to ensure sufficiently large sample sizes even when partitioning the whole simulation into subperiods, we used the longest piControl simulations available (over 700 years). Table 1 displays the 10 models employed for the analysis.

TABLE 1 Summary of the CMIP6 models employed in the study.

Model	Institution	Length (years)	Horizontal res. atmosphere	Reference
CanESM5	CCCma	800	2.8°	Swart et al. (2019)
CESM2	NCAR	1200	1°	Danabasoglu et al. (2020)
FGOALS-g3	CAS	700	2°	Li et al. (2020)
GISS-E2.1-G	NASA GISS	850	2.5°	Kelley et al. (2020)
INMCM5	RAS	1200	2°	Volodin et al. (2017)
IPSL-CM6A-LR	IPSL	1200	2.5°	Boucher et al. (2020)
MIROC6	JAMSTEC	800	1.4°	Tatebe et al. (2019)
MPI-ESM1.2-LR	MPI	1000	1.8°	Gutjahr et al. (2019)
MRI-ESM2.0	MRI	700	1.2°	Yukimoto et al. (2019)
SAM0-UNICON	SNU	700	1.25°	Park et al. (2019)

The variables used in the analysis include mean sea-level pressure (MSLP), sea-surface temperature (SST), 200 hPa zonal and meridional wind components (u200 and v200, respectively) and 200 hPa geopotential height (Z200). Top-of-atmosphere outgoing longwave radiation flux (OLR) was used as a proxy of tropical convective precipitation anomalies. The model data were regridded onto a common regular grid with a 2.5° horizontal resolution. The regridding and computation of the aggregation of the data into ND was performed using Earth System Model Evaluation Tool (ESMValTool) version 2.0 (Righi et al., 2020) and the model data were obtained through the CMIP data pool in the German Climate Computing Center (Deutsches Klimarechenzentrum; DKRZ). Finally, for model evaluation purposes, data from the ERA5 reanalysis (Hersbach et al., 2020), covering the period 1940-2024, were used. The data are produced by the European Centre for Medium Range Weather Forecasts (ECMWF) and have been retrieved from the Copernicus Climate Data Store.

2.2 | Definition of indices

This study employs the Niño 3.4 index (hereafter N34) as the reference metric for characterising ENSO variability. N34 is defined as the area-weighted sea-surface temperature (SST) anomalies over the region (170°W - 120°W, 5°S - 5°N). In this analysis, N34 was standardised and computed based on November-December mean SST data.

In the observations, the East Atlantic Pattern (EAP) emerges as the second leading empirical orthogonal function (EOF) of mean sea-level pressure (MSLP) anomalies in the North Atlantic region (90°W - 40°E, 20°N - 80°N). The associated, standardised, principal component time series is defined as the East Atlantic Index (EA). In order to find the EAP in the CMIP6 models, we performed an EOF analysis in each model over the same spatial domain. The area-weighted spatial covariance between the model's EOFs and the ERA5 EAP was computed, and the EOF that exhibits highest pattern covariance with ERA5 EAP was regarded as the model's EAP. While it is acknowledged that the model's EAP might in some cases differ from the ERA5 reference (reflecting known mean-state biases in individual models), this definition ensures that the identified pattern constitutes a genuine mode of variability within the model's specific climatological state, thereby preserving physical consistency.

2.3 | Methods for teleconnection analysis

The ENSO teleconnection patterns were analysed by means of linear correlation and regression of the anomalies of a specific variable (e.g. MSLP) with N34. The anomalies were computed by subtracting the average of the whole simulation period. Besides, in order to study the interannual signal associated with the ENSO phenomenon, a Butterworth highpass filter was applied to the spatial data, with a cutoff period of 7 years.

On the other hand, the wave propagation pattern associated with stationary Rossby waves is diagnosed with the wave activity flux (WAF), which is a vector that is tangent to the local group velocity of the stationary Rossby wave packets. Takaya and Nakamura (2001) derived the zonal and meridional components of the WAF vector for quasigeostrophic eddies on a zonally varying basic flow in spherical coordinates:

$$W = \frac{p\cos\varphi}{2|U|}\begin{pmatrix} \frac{U}{a^2\cos^2\varphi}\left[\left(\frac{\partial\psi'}{\partial\lambda}\right)^2 - \psi'\frac{\partial^2\psi'}{\partial\lambda^2}\right] + \frac{V}{a^2\cos\varphi}\left[\frac{\partial\psi'}{\partial\lambda}\frac{\partial\psi'}{\partial\varphi} - \psi'\frac{\partial^2\psi'}{\partial\lambda\partial\varphi}\right] \\ \frac{U}{a^2\cos\varphi}\left[\frac{\partial\psi'}{\partial\lambda}\frac{\partial\psi'}{\partial\varphi} - \psi'\frac{\partial^2\psi'}{\partial\lambda\partial\varphi}\right] + \frac{V}{a^2}\left[\left(\frac{\partial\psi'}{\partial\varphi}\right)^2 - \psi'\frac{\partial^2\psi'}{\partial\varphi^2}\right] \end{pmatrix} \tag{1}$$

where φ and λ are the latitude and longitude, p is the pressure normalised by 1000 hPa, a is the Earth's radius, $|U|$, U and V represent the climatological (or basic state) magnitude of the horizontal wind, zonal and meridional component of the wind, respectively, and ψ' represents the geostrophic streamfunction anomaly or perturbation with respect to climatology. The WAF defined this way is a horizontal vector, and its direction is parallel to the local group velocity of the stationary Rossby wave packet. Since φ tends to 0 as we approach the equator, the WAF is only computed and shown for latitudes higher than 20°.

2.4 | Assessment of non-stationarity and its associated dynamical mechanisms

Initially, we assessed the stationary component of the teleconnection based on the regressions and correlations across the full simulation period, omitting subperiod distinctions. Subsequently, we evaluated the non-stationary component with the linear correlation coefficient between EA and N34, computed in moving 21-year time windows. Note that the sample correlation coefficient will exhibit variability even if the teleconnection itself was stationary, yielding an apparent non-stationarity simply due to sampling uncertainty. Therefore, it is relevant to evaluate whether the sample correlations feature significantly larger variability than would be expected if the teleconnection was stationary. To this purpose, we followed the linear stochastic model approach from Rieke et al. (2021), which consists of representing the EA index as a term that is linear with N34 (the α coefficient in Equation 2) and another term that represents a white noise process (ε in Equation 2).

$$EA = \alpha \cdot N34 + \varepsilon, \tag{2}$$

where EA, $N34$ and ε are time-series vectors. Under the assumption that the null hypothesis H0:"the teleconnection itself is stationary" is true, α is time-independent and a theoretical distribution of the sample correlation between EA and N34 can be built with the stochastic model. In order to build this distribution, first the α coefficient is computed as the Pearson correlation coefficient between EA and N34 using the full-length data from the specific CMIP6 model,

while $\varepsilon = \varepsilon(t)$ is obtained from randomly sampling, for each t, from a normal distribution with zero mean and $\sqrt{1-\alpha^2}$ standard deviation, which ensures that the standard deviation of the resulting EA time series is very close to unity. By considering 5000 realisations of $\varepsilon(t)$, we obtained 5000 realisations of the EA time series exhibiting a full-period correlation close to α. Then, in the same way as with the CMIP6 simulation, the 21-year moving correlation between EA and N34 was computed for all the realisations of the stochastic model, and the variability of the 21-year correlation between the stochastic model realisations and the CMIP6 model are compared. The p-value was finally estimated as the fraction of stochastic model realisations yielding a larger variability of the sample correlation than the observed one in the CMIP6 model.

Furthermore, in the assessment of the multidecadal variability of the teleconnection, we defined two different periods: periods with positive, significant (p-value < 0.05) EA-N34 correlation were labelled as POSCORR, while periods with a weak EA-N34 correlation were labelled as WEAKCORR. In order to determine what specific years go into POSCORR and WEAKCORR, the 21-year moving correlation between EA and N34 was used. If the correlation within a given window is positive and statistically significant, all years contained in that window were included in POSCORR, while years contained within windows that feature correlations lower than 0.2 and not included in POSCORR went into the WEAKCORR sample. Defining the periods in this objective way ensures sufficiently large sample sizes in both periods as well as a clear separation between the samples.

The analysis of dynamical mechanisms associated with the multidecadal variability of the teleconnection involved the examination of differences in the linear regression patterns onto N34 (computed as the regression pattern in POSCORR minus that of WEAKCORR) together with differences in the climatology. In order to highlight the common signal across the models, the discussion mainly focuses on the multi-model mean of the subset of models exhibiting significant multidecadal variability, rather than on the individual model results.

2.5 | Statistical significance

To evaluate the robustness of a signal — whether a difference in composite climatologies or a difference in ENSO regression patterns — we compared it against the sampling variability expected from the same calculation applied to randomly resampled groups of years. We pooled all years contributing to the POSCORR and WEAKCORR samples and iteratively (5000 times) drew random pairs of samples of the same sizes as the original groups, without replacement, recomputing the statistic of interest (e.g. a composite climatological difference, or a difference in ENSO regression patterns) for each random pair. This yields a null distribution of values expected by sampling variability alone. Finally, the proportion of resampled values at least as extreme as the actual observed value in the CMIP6 model provides an empirical p-value. Rather than performing this analysis at every grid point, we focused on large-scale features likely relevant to the teleconnection.

3 | RESULTS

3.1 | Stationary component of the ENSO early-winter teleconnection in CMIP6

As a starting point, we analyse the ENSO-associated anomalous MSLP patterns in the North Atlantic in early winter in the whole simulation period for each model, without distinguishing any subperiods (Figure 1a). This initial assessment offers an overview of the stationary (or most stable in time) component of the teleconnection. The MSLP regression

patterns vary across models, highlighting some degree of uncertainty in the MSLP response to ENSO in the North Atlantic, although there is a signal common to almost all of them consisting of negative MSLP anomalies centred close to western Europe. The multi-model mean (MMM) pattern reflects this common response and shows a spatial pattern that somewhat aligns with the EAP. The values of the linear correlation coefficient between EA and N34 computed using the full simulation period (displayed in the bottom right boxes in Figure 1a) throughout the entire period are statistically significant in 7 out of the 10 models, although the critical correlation values for statistical significance are low due to the very large sample sizes. For context regarding the observed teleconnection pattern, the regression pattern using the ERA5 reanalysis data from 1940 to 2024 is also shown. The observed pattern in the ERA5 reanalysis shows an area of negative MSLP anomalies centred to the south of Iceland and west of the British Isles, with a correlation of 0.47 between EA and N34 (p-value < 0.00001), in accordance with studies that showed that ENSO mainly affects the EAP in early winter (King et al., 2018; Ayarzagüena et al., 2018; Geng et al., 2023). Comparing the CMIP6 regression patterns with the ERA5 one, the models appear to broadly capture the spatial pattern of MSLP anomalies associated with ENSO. However, an underestimation of the MSLP anomalies and the correlation coefficient between EA and N34 can be clearly noted in all of them. While this could be an indication of model biases or deficiencies in the representation of some of the teleconnection processes, it could also well arise from comparing two samples with very different sizes (n=85 for ERA5 versus n>700 for CMIP6 models). In order to reject the null hypothesis that this difference is due to sampling uncertainty, 10000 random samples of size n=85 (the same as the ERA5 one) are drawn from each CMIP6 model simulation, and the correlation between EA and N34 is computed in each of the random samples, yielding a distribution of possible values of the correlation coefficient in the model. The result of this analysis shows that, in all the models, the ERA5 value lies in the extreme right tail of the distribution. If the distributions of all the models are combined to build a multimodel distribution (shown in Figure 1b), the probability of sampling a correlation higher than or equal to the ERA5 value is less than 0.1%. This provides strong support that, despite capturing the spatial pattern reasonably well, CMIP6 models significantly underestimate the magnitude of the ENSO-EAP teleconnection in early winter. The underestimation of the magnitude of ENSO teleconnection patterns is a widely reported issue that affects multidecadal GCM models (Ayarzagüena et al., 2018; Molteni et al., 2020) as well as state-of-the-art seasonal forecasting systems (Abid et al., 2023; O'Reilly, 2025).

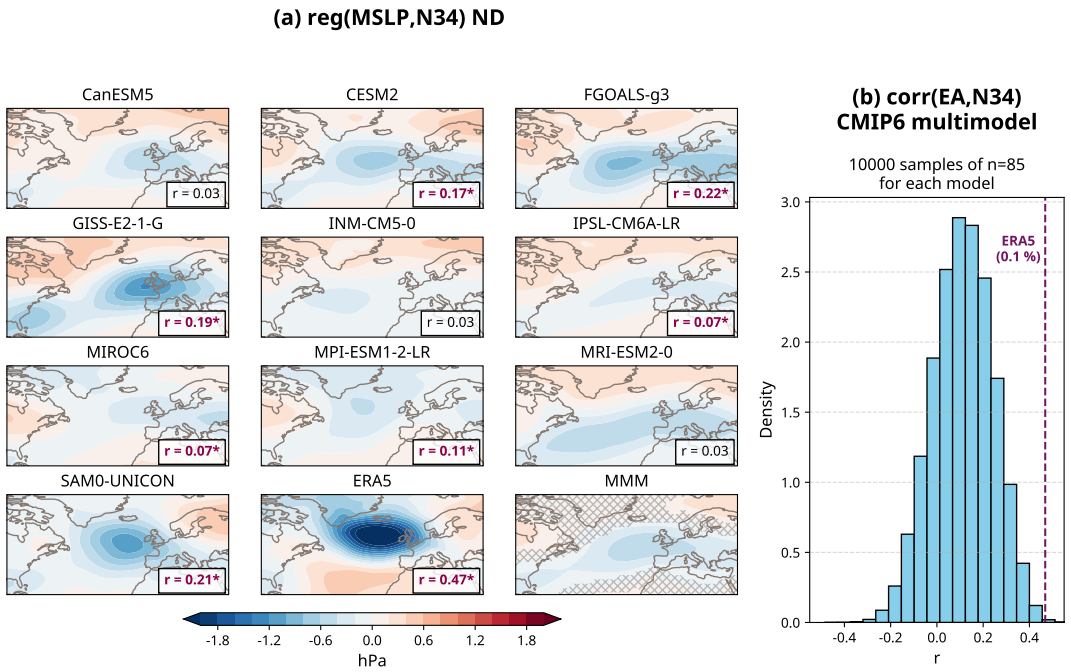


FIGURE 1 (a) Regression of MSLP anomalies onto N34 in the piControl simulations of CMIP6 models and in ERA5 (shading; hPa). The Pearson correlation coefficient between EA and N34 in the whole period (entire simulation in CMIP6 runs and 1940-2024 in ERA5) is displayed in the lower right corner of each subplot. Correlation values for which p-value ≤ 0.05 are highlighted. The unhatched regions in the MMM represent where at least 75% of the models agree on the sign of the anomaly. (b) Histogram showing the distribution of the Pearson correlation coefficient between EA and N34 in random samples with the same size as the ERA5 sample. 10000 random samples were used in each CMIP6 model and the distributions of all the models were combined into a single one. The dashed vertical line represents the ERA5 value.

3.2 | Multidecadal variability of the teleconnection

We now analyse how the correlation between ENSO and the EAP has changed across different multidecadal periods throughout each of the simulations. A remarkable variability of the ENSO-EAP teleconnection can be noticed in all the models, where the 21-year moving correlation between EA and N34 can take a wide range of values (Figure 2, shaded density plots). Remarkably, just as periods of statistically significant positive correlation are observed, periods of statistically significant negative correlation also occur. Nevertheless, considering the data from all the models, periods with positive significant correlation are about 6 times more frequent than the periods with negative significant correlation, reflecting the fact that most of the distributions are displaced towards positive correlations. These results remain qualitatively similar if other time window sizes are used (not shown).

The link between ENSO and the EAP exhibits notable multidecadal variability in the CMIP6 models, but we note that this could well occur even if the teleconnection itself was stationary — just due to sampling uncertainty — which would yield an "apparent" non-stationarity of the teleconnection. Hence, the next question worth addressing is: can the

variability of the correlation between EA and N34 be explained just by sampling uncertainty or is there a significant non-stationarity of the teleconnection emerging? This is the starting point to employ the linear stochastic model framework presented in the Data and Methods section (Rieke et al., 2021). The comparison of the distributions of the 21-year correlation between EA and N34 of CMIP6 models with the stochastic model distribution (red-dotted density plots in Fig. 2) allows rejection of the null hypothesis in 5 of the models (FGOALS-g3, GISS-E2.1-G, IPSL-CM6A-LR, MPI-ESM1.2-LR and MRI-ESM2.0). This result suggests that there is a significant chance that the ENSO early-winter teleconnection to the North Atlantic exhibits meaningful multidecadal variability, supporting the non-stationarity hypothesis raised from observational studies (Hou et al., 2023; Fernández-Castillo et al., 2025).

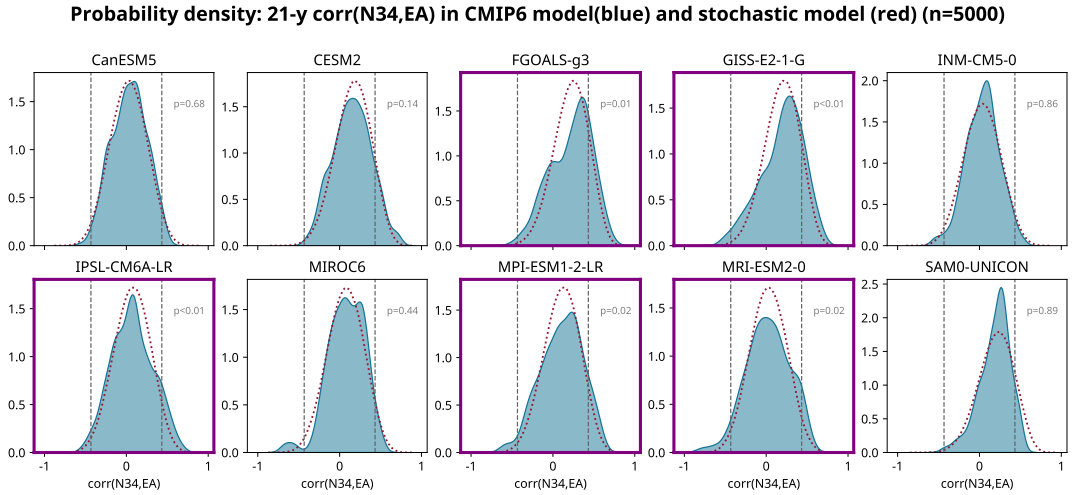


FIGURE 2 Probability density plots of the Pearson correlation coefficient between N34 and EA indices in moving 21-year windows for each model (blue). The density plots corresponding to the 5000 realisations from the stochastic model with a stationary teleconnection (see Methods) are shown with a red dotted line. The highlighted subplots correspond to the models showing a statistically significant multidecadal variability (i.e. the p-value for the the null hypothesis of a stationary teleconnection, displayed in grey in each subplot, is less than 0.05), and the vertical grey lines show the statistical significance threshold (p-value 0.05) values for the 21-year sample correlation coefficient.

Next, we focus on what the ENSO-associated MSLP patterns are in the periods with strong ENSO-EAP correlation (POSCORR periods, see Methods) and periods with an inactive ENSO-EAP teleconnection (WEAKCORR periods, see Methods) in the models that exhibit significant multidecadal variability. The anomalous negative MSLP centre associated to the positive phase of the EAP emerges as a robust response to El Niño in POSCORR (Figure 3, left column), in a stronger way than when using the full simulation period (Figure 1) and in closer agreement with the ERA5 reference in 1940-2024. In this way, the positive phase of the EAP is favoured under El Niño conditions, while the negative phase is favoured in La Niña. Nevertheless, it is interesting to observe the differences between the models in the North Atlantic and in other regions outside from the North Atlantic. Focusing first in the North Atlantic region, the shape and orientation of the negative MSLP centre characteristic of the EAP varies across the different models, which would result in somewhat different impacts on surface air temperature and precipitation in western Europe. Furthermore, turning our attention upstream in the North Pacific, different responses are observed regarding the Aleutian low. The Aleutian low is one of the most prominent features of the ENSO extratropical teleconnection, with a stronger low

being favoured in El Niño while a weaker one being favoured in La Niña. While all the models capture this general behaviour, some inter-model spread can be observed. These differences in the teleconnection pattern upstream can be relevant to the teleconnection to the North Atlantic due to the role of eddy energy propagation from North America into the North Atlantic as a tropospheric pathway of the ENSO teleconnection (O'Reilly et al., 2024).

In contrast, the MSLP regression patterns onto N34 in periods with an inactive ENSO-EAP teleconnection (WEAKCORR periods) show very weak signals in the North Atlantic with limited cross-model agreement (Figure 3, middle column). However, we note that the WEAKCORR periods are herein defined as periods with inactive ENSO-EAP teleconnection. Therefore, this definition does allow other teleconnection patterns to be featured in WEAKCORR, such as a teleconnection to the NAO, or to the Scandinavian pattern. Thus, two plausible situations feasibly explain the weak signals in WEAKCORR: a) in WEAKCORR periods the teleconnection to the North Atlantic is just too weak for a signal to emerge, or b), in WEAKCORR, ENSO also features robust teleconnections to other modes of circulation (e.g. NAO or Scandinavian pattern), but none of these teleconnections prevail and therefore the overall signal after averaging across the WEAKCORR periods is weak. As an example, GISS-E2.1-G and, to a lesser extent, FGOALS-g3 and MRI-ESM2.0, feature a signal on the ENSO-regressed MSLP pattern in WEAKCORR that is somewhat similar to the NAO, indicating that, when ENSO does not affect the EAP, it mainly affects the NAO. Once again, it is worth highlighting some differences found upstream and in particular over the North Pacific, although the lack of cross-model agreement attenuates this signal in the multimodel mean (bottom right subplot in Figure 3). These differences are particularly visible in FGOALS-g3 and MRI-ESM2.0. Nevertheless, it will be shown later that these differences emerge more clearly when analysing the wave structure in the upper troposphere.

In summary, the ENSO-regressed MSLP patterns reveal a robust ENSO-EAP teleconnection in POSCORR while a lack of a strong signal in WEAKCORR. This is somewhat logical by construction of the windows, but puts forward the existence of a non-stationary signal, with periods in which the ENSO-EAP is robust (POSCORR) and other periods in which it may not be observed at all (WEAKCORR), a feature that agrees with Hou et al. (2023) and Fernández-Castillo et al. (2025).

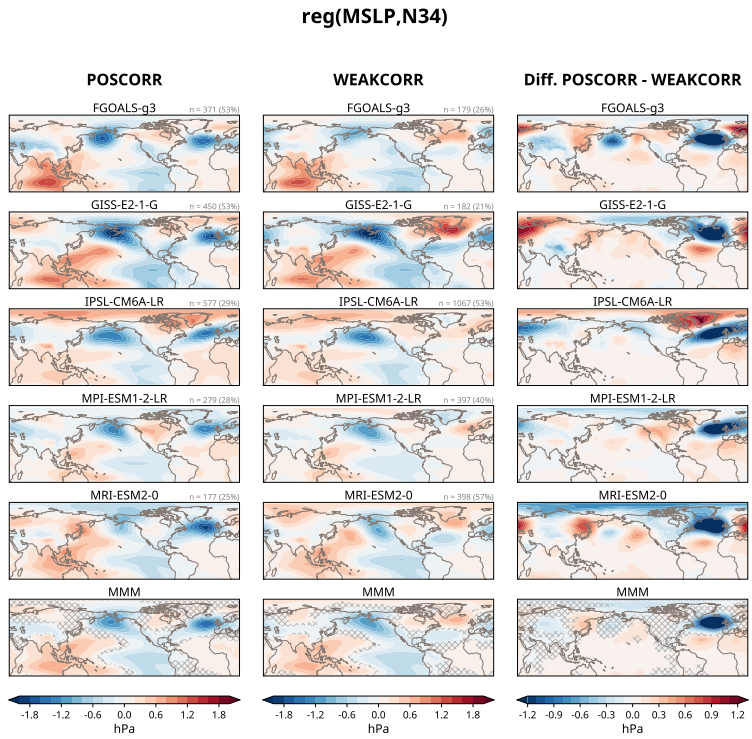


FIGURE 3 Linear regression maps of MSLP anomalies onto N34 (shading; hPa) in the periods with strong ENSO-EAP teleconnection (POSCORR; see Methods; left column), in the periods exhibiting weak ENSO-EAP teleconnection (WEAKCORR; middle column) and difference (POSCORR minus WEAKCORR; right column), for the subset of models exhibiting significant multidecadal variability. The value of *n* in the upper right corner displays the sample size and the % relative to the size of the full simulation. The unhatched regions in the multimodel mean (MMM; bottom row) represent where at least 4 out of the 5 models agree on the sign of the anomaly.

The tropospheric pathways of the teleconnection also exhibit several relevant differences between POSCORR and WEAKCORR in the models with significant multidecadal variability. The regression of Z200 anomalies onto N34 and the associated WAF field in both periods provides an initial overview of the changes in the tropospheric pathways regarding the stationary Rossby wave response, serving as a foundation for the more detailed analysis that follows in the next section, which will cover the dynamical mechanisms.

The Z200 regression patterns show the characteristic Gill-type response over the tropical Pacific (Gill, 1980) and negative anomalies around the Aleutian low region (Figure 4a,b). The anomalies over the North Pacific and North America approximately map onto the Pacific-North America pattern, which is known to be linked with ENSO variability. However, the WAF vectors reveal stronger wave energy emanating from the Indian Ocean region and propagating northeastward into the North Pacific in POSCORR, while this wave activity is weaker in WEAKCORR. We also observe a slightly stronger Gill response in POSCORR, which could be reflecting stronger convection anomalies in the eastern tropical Pacific. Indeed, the WAF vectors also reveal a slightly stronger wave activity emanating from the eastern tropical Pacific in POSCORR compared to WEAKCORR. The difference in the Z200 regression shows the strongest

anomalies over the North Atlantic, which is expected by construction (Figure 4c). However, it is interesting to inspect the changes upstream as these can have an impact in the North Atlantic. The most remarkable feature is a wave-like pattern over East Asia into the North Pacific and North America, which aligns very closely with the wavenumber-3 pattern associated with pure Indian Ocean convection anomalies (i.e. with the effects of ENSO removed) (Abid et al., 2021) and an associated wave source in southeast Asia (Sabatani and Gualdi, 2025) in early winter. This strongly suggests that the changes in the Indian Ocean pathway could be playing a primary role in the changes in the teleconnection patterns between POSCORR and WEAKCORR. Changes in the Indian Ocean pathway can lead to modulations of the jet stream and storm track response to ENSO in the North Pacific, which subsequently affect the propagation of eddy energy into North America and ultimately, into the North Atlantic region. Even though the differences upstream of the North Atlantic are not particularly strong, small displacements of the jet and storm track in the North Atlantic entrance region can result in the eddy-mean flow feedbacks shaping up a notably different teleconnection pattern.

In principle, these results suggest that the strength of the Indian Ocean/East Asia pathway has an influence the ENSO teleconnection to the North Atlantic. This result agrees with previous studies showing the important role of the Indian Ocean pathway as one of the main tropospheric pathways involved in the ENSO early-winter teleconnection to the North Atlantic (Mathieu et al., 2004; Joshi et al., 2021; Abid et al., 2021, 2023), and we will now examine these mechanisms in more detail.

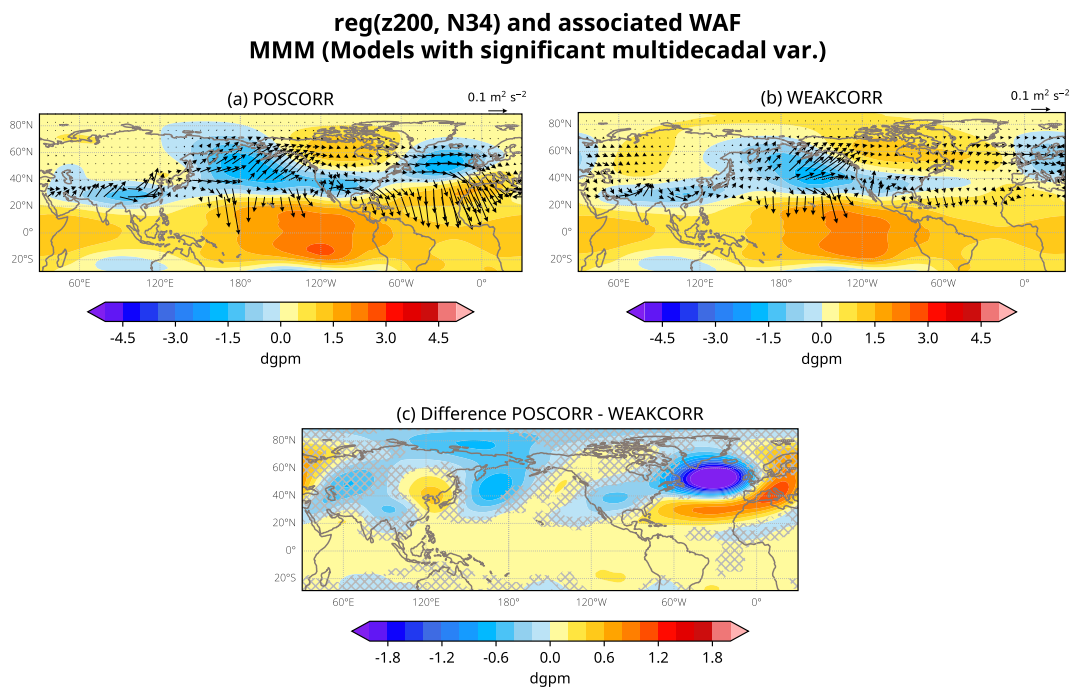


FIGURE 4 Linear regression maps of Z200 anomalies onto N34 (shading; dgpm) and associated WAF (vectors; m^2s^{-2}) in ND for the multimodel mean of the models featuring significant multidecadal variability in (a) POSCORR and (b) WEAKCORR. The difference between POSCORR and WEAKCORR is shown in (c), with the unhatched regions representing where at least 4 out of the 5 models agree on the sign of the anomaly.

3.3 | Dynamical mechanisms related to the multidecadal variability

The analysis so far has revealed that the ENSO early-winter teleconnection to the North Atlantic exhibits multidecadal variability in the CMIP6 piControl simulations, and that there is a substantial chance that it is not a purely stochastic feature, but likely driven by some dynamical mechanisms. Hence, it is worth examining what those mechanisms are. On the one hand, the teleconnection may change due to alterations in the generation of Rossby waves, to which changes in the tropical convection patterns and climatological u200 are relevant. On the other hand, changes in the propagation of the Rossby waves generated from ENSO-related sources can also lead to a different teleconnection pattern.

Thus, in the subsequent analysis, we examine changes in the tropospheric pathways of the teleconnection. Since our interest lies in identifying the mechanisms responsible for a substantial multidecadal modulation of the teleconnection, the analysis will mainly focus on the subset of models for which such modulation is statistically significant, and in particular the multi-model mean of these models, in order to isolate dynamical features common across them. In any case, results for all individual models are presented in the Supporting Information, including those without significant multidecadal variability.

Tropical convection patterns during ENSO events have a strong influence on which regions are prone to act as sources of Rossby waves in the teleconnection. Hence, we begin by analysing the anomalous OLR field (used as a proxy of tropical convection anomalies) associated with ENSO in POSCORR and WEAKCORR. Remarkably, the OLR regressions onto N34 in POSCORR and in WEAKCORR reveal changes in these tropical convection patterns (Figure 5a). The most prominent differences between the POSCORR and WEAKCORR regression patterns are found over the Indian Ocean region, with a clear dipole signature. These anomalies featured in the difference of regressions have the same sign as the "base" regression pattern onto N34 (not shown), suggesting that the dipole becomes stronger in POSCORR and weaker in WEAKCORR. Comparing the observed dipole signal (area-average of blue box minus the area-average of red box in Figure 5a) with the null distributions obtained by sampling variability alone, we see that it falls in the tail of the distribution in most of the models, suggesting that this represents a robust signal which stands out from sampling variability. The stronger dipole over the Indian Ocean in POSCORR is consistent with the stronger stationary Rossby wave activity emanating from that region, suggested by the anomalous Z200 field and associated WAF vectors in Figure 4. Further analyses based on partial regression (not shown) reveal that the wave-like structure appearing over East Asia in Figure 4c can be readily related to the OLR dipole over the Indian Ocean, in agreement with Abid et al. (2021). This Indian Ocean convection feature is particularly strong in the MRI-ESM2.0 model (Figure S1), which in turn shows a clearer wave structure emanating from the Indian Ocean and East Asia into the North Pacific (Figure S2). We note that, using historical runs from CMIP6 models, Sabatani and Gualdi (2025) showed that models exhibiting a stronger wave source over southeast Asia — linked to convection anomalies over the tropical Indian Ocean — generally feature a stronger ENSO-EAP teleconnection in December in comparisson to those featuring a weaker source. Our results show that, within a model, the periods that feature stronger tropical Indian Ocean convection anomalies — which contribute to enhanced upper-level divergence and to a stronger southeast Asia wave source — tend to feature a stronger ENSO-EAP teleconnection.

Another region of interest is the Gulf of Mexico and Caribbean Sea. According to previous studies, a Rossby wave source over this region can trigger a wavenumber 3 pattern in the North Atlantic which can favour an EAP (Ayarzagüena et al., 2018; Hardiman et al., 2019; Sabatani and Gualdi, 2025). Indeed, an OLR signal can be found over this

region although with a notably weaker magnitude than in the Indian Ocean. It could be argued that these differences over the Caribbean may be appearing by construction, due to the EAP itself driving convection anomalies in this region in POSCORR while in WEAKCORR there is no EAP and therefore no convection anomalies are favoured. However, the regression of OLR anomalies onto EA in WEAKCORR reveals very weak OLR signals in the Gulf of Mexico and Caribbean Sea region (Figure S3). In other words, convection anomalies in the Gulf of Mexico and Caribbean Sea region are not necessarily caused by an EAP. This suggests that the stronger convective activity found in the Gulf of Mexico and Caribbean region in POSCORR indeed represents a meaningful signal which could be further contributing to an EAP teleconnection. Additionally, some signals in the OLR difference are present over the equatorial Pacific, although these are weaker than the ones previously discussed and in general with no clear consensus among the models. Finally, while individual model analyses reveal a high degree of uncertainty (Figure S1), likely related to model-specific biases in the representation of tropical convection patterns, most models exhibit signals in the key regions, namely the tropical Indian Ocean, tropical Pacific and Gulf of Mexico-Caribbean Sea.

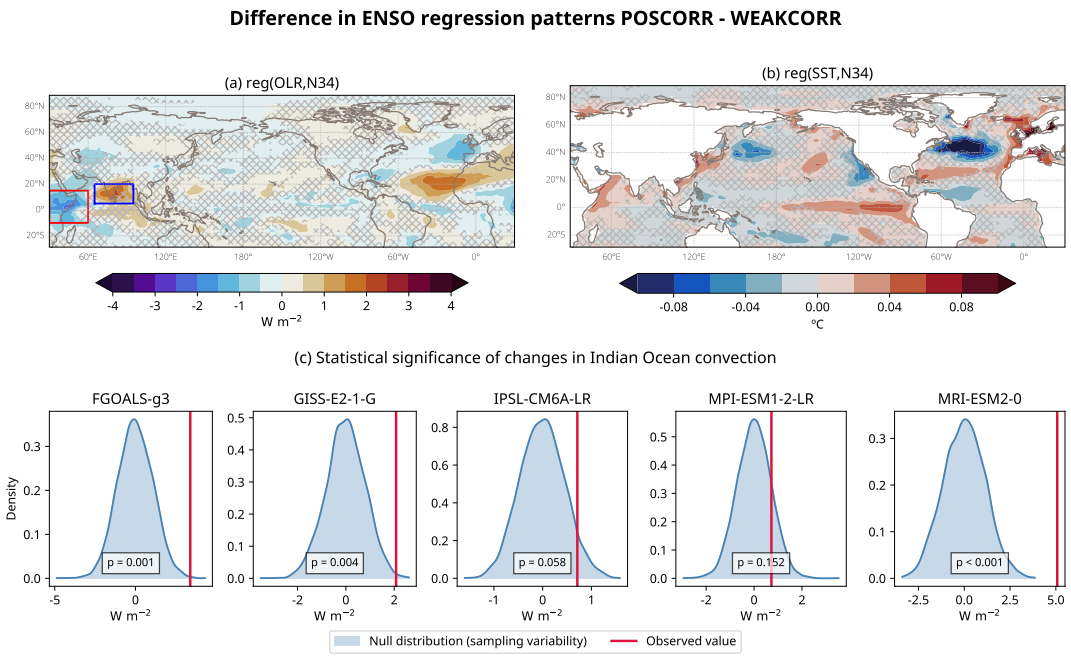


FIGURE 5 Difference in the linear regression maps (computed as POSCORR minus WEAKCORR) of (a) OLR and (b) SST anomalies onto N34 (shading; W m^{-2} and °C, respectively), for the multimodel mean of the models exhibiting significant multidecadal variability. The unhatched regions represent where at least 4 out of the 5 models agree on the sign of the anomaly. (c) Empirical probability density functions (blue) showing the null distribution of values of the Indian Ocean convection dipole signal (obtained by taking the difference between the area average of the blue box minus the area average of the red box in (a)) obtained by sampling variability, following the procedure explained in the Methods section. The red vertical line shows the observed value in the CMIP6 model and the estimated p-value is displayed at the bottom.

Aiming to understand the stronger tropical convection activity in POSCORR, differences in the regression patterns of SST onto N34 are analysed for the multimodel mean of the models with significant multidecadal variability (Figure

5b), while individual model results are displayed in Figure S4. The Indian Ocean Dipole (IOD) frequently co-occurs with ENSO and peaks between September and October, although IOD variability can exist independently from ENSO (Abid et al., 2021). Thus, regression patterns of SST anomalies onto N34 usually also feature SST anomalies over the Indian Ocean, with warm anomalies in the west of the Indian Ocean basin and cold anomalies over Indonesia and Australia, corresponding to a positive phase of the IOD. The difference in the regression patterns between POSCORR and WEAKCORR shows a similar signature to that of the +IOD phase, suggesting that the SST dipole becomes stronger in POSCORR than in WEAKCORR, which aligns with the enhanced OLR response discussed earlier. It could be argued that the SST anomalies over the Indian Ocean may be appearing as a result of downstream propagation of circulation anomalies from the North Atlantic region. However, analysis of October SST shows a similar dipole signal, with a stronger magnitude of the anomalies close to Indonesia (Figure S5), providing more confidence that the convection anomalies over the Indian Ocean are more a cause rather than an effect explaining the stronger EAP in the North Atlantic. Furthermore, there is no clear wavetrain pattern connecting the geopotential height anomalies in the North Atlantic with the Indian Ocean and East Asia region, which is explained by the disjointed jet stream structure in the eastern North Atlantic (e.g. Figure 6a), which hinders the propagation of Rossby waves from the North Atlantic into the Indian Ocean.

The difference of regressions of SST also shows a warm signal over the eastern equatorial Pacific, indicating a favourability towards eastern Pacific ENSO events in POSCORR, although the exact pattern varies notably across models (Figure S4). Previous studies have found that eastern Pacific ENSO events are usually more correlated to the IOD than central Pacific ones (Zhang et al., 2015; Fan et al., 2017), so it is likely that the SST signal in the eastern equatorial Pacific is related, to some extent, to the OLR anomalies over the Indian Ocean (Figure 5a). Regarding the strong signals in the North Atlantic, it should be noted that these are mainly appearing as a result of the circulation anomalies related to the EAP.

Apart from changes in the ENSO spatial pattern, changes in the generation of Rossby waves relevant to the teleconnection can also arise from changes in the tropical SST variability. The ratio of variances of SST between POSCORR and WEAKCORR does not reveal any clear signals over the tropical Pacific, with a lack of cross-model agreement (Figure S6). However, some signal emerges over the Indian Ocean, where the values greater than 1 indicate that the variability of SST there is stronger in POSCORR compared to WEAKCORR, although with limited cross-model agreement. There is also a weak signal of POSCORR periods exhibiting enhanced SST variability over the Caribbean Sea, although again the cross-model agreement is limited. Hence, no robust conclusions can be drawn regarding whether the change in the teleconnection is caused by a stronger variability of ENSO in POSCORR. Nevertheless, it is possible that the enhanced SST variability over the Indian Ocean partially contributes to enhance the convective activity in the area (as could be seen in the regressions with OLR). This would contribute to a stronger wave activity into the North Pacific and North America in a way that favours an ENSO-EAP teleconnection.

Thus far, the analysis of ENSO-regressed patterns suggests that the multidecadal variability of the early-winter teleconnection can be at least partially explained by changes in the ENSO-associated tropical convection patterns, which affect the upper-level divergence and the regions prone to act as sources of Rossby waves. Nevertheless, we also need to analyse changes in the mean state or climatology, since these can have an effect on the propagation of Rossby waves from tropical regions towards the extratropics (Hoskins and Karoly, 1981). Hence, the subsequent analysis focuses on identifying changes in the mean state that could be relevant to the tropospheric pathways to the North Atlantic.

Changes in the climatology of u200 can be observed, with the strongest signals over the North Pacific. The climatological upper-level flow plays a vital role in the propagation of stationary Rossby waves in ENSO teleconnections to the extratropics as it determines whether the waves are reflected or refracted, thus determining the trajectory of the waves (Hoskins and Karoly, 1981). Climatologically, u200 shows a belt of westerly winds spanning the subtropics and mid-latitudes (contours in Figure 6a). This structure is not zonally symmetric, as it features two clear maxima in the mid-latitudes in the western boundaries of the major ocean basins: a primary core off the East Asian coast and a secondary core over eastern North America and the western North Atlantic. In POSCORR, there is an intensification of the westerlies over the Bering sea, which is northeast of the primary u200 maximum, while there is a weakening of u200 south around 30°N, 160°W (shading in Figure 6a). Overall, the u200 climatology difference indicates that the North Pacific jet stream is shifted slightly poleward over the North Pacific and the jet maximum is elongated, extending further to the east. This u200 climatology difference pattern over the North Pacific is remarkably similar to the u200 bias pattern shown in Sabatani and Gualdi (2025), where models with an equatorward-shifted climatological North Pacific jet stream fail to simulate an ENSO-EAP teleconnection in December. In those models, the described biases in the North Pacific jet affect the propagation of waves emanating from the southeast Asia and tropical Pacific regions. A similar circumstance also affects state-of-the-art seasonal forecasting systems (O'Reilly, 2025). Moreover, in observations, equatorward shifts in the North Pacific jet and storm track tend to reduce the frequency of poleward jet excursions in the North Atlantic, which are crucial for shaping up the seasonal-mean circulation anomalies in response to ENSO there (O'Reilly et al., 2024). Hence, it is likely that the change in u200 climatology between POSCORR and WEAKCORR — characterised by the poleward displaced and eastward extension of the strong u200 —contributes to a more efficient propagation of waves into North America in POSCORR, as displayed in the WAF field (Figure 4). Apart from this feature in the North Pacific, there is a weakening signal just south of the South Asian jet. This region is important as convection anomalies close to the Indian Ocean and East Asia are a relevant source of upper-level divergence, and the generation of Rossby waves and their propagation can be notably affected by this u200 maximum. This weaker South Asian jet in POSCORR, together with the enhanced Indian Ocean precipitation dipole, feasibly explain the stronger propagation of Rossby waves especially in East Asia (close to 120°E), where no significant weakening of u200 is observed. Nonetheless, it is noted that individual models display a high degree of uncertainty in the signal of u200 (Figure S7), which are likely explained to a certain extent by the model-specific biases in the representation of the climatological jet stream.

The SST climatology difference between POSCORR and WEAKCORR (Figure 6b) shows very few regions with consistent anomalies across the models, which is revealed by the wide range of signals when comparing individual models (Figure S8). Hence, most of the regions are hatched in the multi-model mean (Figure 6b), meaning that there is no clear consensus regarding the sign of the difference. We find a generalised warm signal in the North Atlantic, but this is mainly contributed just by the IPSL-CM6A-LR model. This model did not show any significant signals of changes in the tropical convection over the Indian Ocean between POSCORR and WEAKCORR, suggesting that in this particular model the multidecadal variability appears to be mainly arising from changes in the extratropical background state. Nevertheless, the strongest signal of SST climatology change is found over the North Pacific, in a region close to 40°N and west of 180°W (close to the Kuroshio extension region, the region with strongest variability). On a broader scale, the pattern over the North Pacific resembles to some extent the negative phase of the Pacific Decadal Oscillation (PDO). In fact, the SST climatology in POSCORR features a pattern that resembles the negative phase of the PDO and the positive phase in WEAKCORR (not shown). This PDO-like signal emerges clearly in two models with significant multidecadal variability: the MPI-ESM1.2-LR and MRI-ESM-2.0 models (Figure S8), which also show stronger differences in the u200 field (Figure S7). The change in the meridional SST gradient in the extratropical North Pacific is statistically significant in most of the models, and especially robust in the MPI and MRI models (Figure 6c). These SST

signals are consistent with Sabatani and Gualdi (2025), where models exhibiting SST biases resembling the pattern shown in Figure 6b in the North Pacific, tend to feature a weak ENSO-EAP teleconnection. Furthermore, despite being weak, these signals from the piControl simulations are also consistent with the fact that, in the last decades, the ENSO-EAP relationship has been observed to be stronger in the negative phase of the PDO while weaker in the positive phase (Fernández-Castillo et al., 2025). While it is acknowledged that this could be coincidental, it does provide additional support that the low-frequency variability of extratropical SST in the North Pacific is probably influencing the ENSO teleconnection to the North Atlantic in early winter.

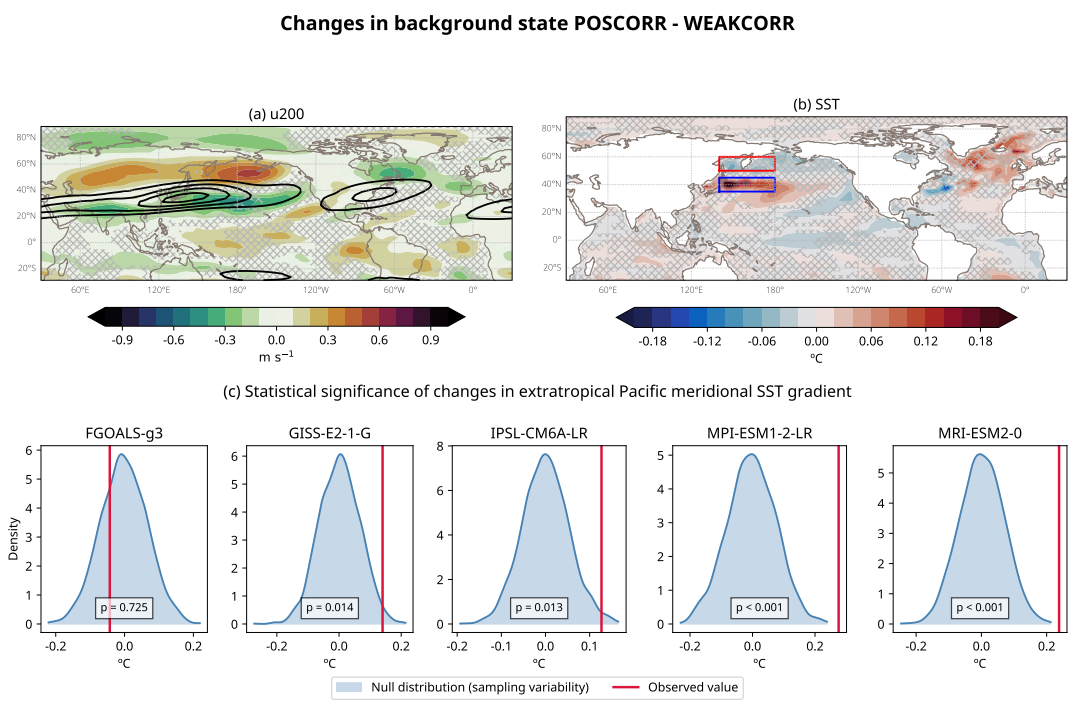


FIGURE 6 Difference in the composite means (computed as POSCORR minus WEAKCORR) of (a) u200 and (b) SST (shading; m s^{-1} and °C, respectively), for the multimodel mean of the models exhibiting significant multidecadal variability. In (a), the u200 climatology of WEAKCORR is displayed in contours, starting from 30 m/s and with a contour interval of 10 m/s. The unhatched regions represent where at least 4 out of the 5 models agree on the sign of the anomaly. (c) Empirical probability density functions (blue) showing the null distribution of values of the meridional SST gradient in the extratropical North Pacific (obtained by taking the difference between the area average of the blue box minus the area average of the red box in (b)) obtained by sampling variability, following the procedure explained in the Methods section. The red vertical line shows the observed value in the CMIP6 model and the estimated p-value is displayed at the bottom.

4 | SUMMARY AND DISCUSSION

In the present study, the early-winter ENSO-EAP teleconnection has been analysed in a set of piControl simulations of models participating in CMIP6. The simulations employed here — over 700 years in length and with approximately

constant external forcings — have provided a suitable framework to robustly assess the multidecadal variability of the teleconnection and plausible modulations related to natural low-frequency variability, in contrast to the short instrumental record.

When analysing the teleconnection using the simulation period as a whole, circulation anomalies somewhat resembling the EAP were found in the North Atlantic, showing that, within these models, the prevalent (or most stable in time) early-winter ENSO teleconnection is the EAP. However, as found in the observational record, the ENSO-EAP teleconnection is stronger in some epochs while non-existent in others (Hou et al., 2023; Fernández-Castillo et al., 2025). Remarkably, there is a significant probability that the multidecadal variability of the teleconnection is statistically significant and not explained just by sampling variability, something that could not be addressed in the observational studies.

The different mechanisms that potentially contribute to the multidecadal variability of the teleconnection are summarised below and illustrated in the schematic in Figure 7:

- Stronger ENSO-related convection anomalies over the Indian Ocean enhance upper-level divergence, which provides a source of Rossby waves and contributes to a stronger wave activity flux into the extratropical Pacific consistent with (Abid et al., 2021; Sabatani and Gualdi, 2025). The wave activity from the Indian Ocean also originates further east due to a weakening of the South Asian jet on its western flank, meaning that the source of Rossby waves is displaced to the east and closer to the Pacific. Overall, this favours an ENSO-EAP teleconnection.
- Changes in the climatological jet stream over the North Pacific affect the propagation of waves through the North Pacific into North America. A northward displaced and more zonally elongated jet stream in the North Pacific increases the wave activity from the Pacific and Indian Ocean pathways into North America and subsequently into the North Atlantic, contributing to an ENSO-EAP teleconnection.
- The negative phase of the PDO is more clearly associated with the ENSO-EAP teleconnection than the positive phase. This is consistent with an observational study which highlighted that, in the last decades, the ENSO-EAP teleconnection is significant in negative PDO phases while not significant in the positive PDO phase (Fernández-Castillo et al., 2025).

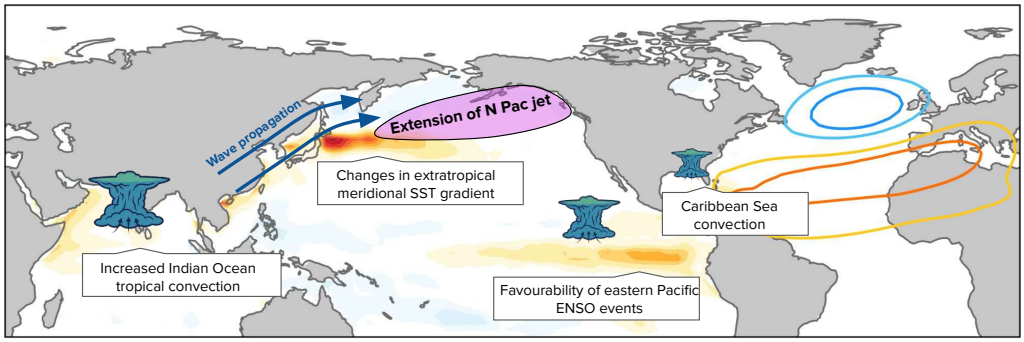


FIGURE 7 Schematic diagram illustrating the main mechanisms contributing to the multidecadal variability of the ENSO-EAP teleconnection in CMIP6 piControl simulations. The shading represents SST anomalies and the contours show the anomalous 200 hPa geopotential height field in the North Atlantic. Note that these fields are purely schematic and represent qualitative patterns rather than actual physical magnitudes.

While most of these signals are weak in magnitude, they are robust enough to stand out clearly from sampling variability. Moreover, they also align with other observational and model-based analyses that highlighted the roles of the Indian Ocean and the Gulf of Mexico and Caribbean Sea as relevant pathways in the ENSO early-winter teleconnection to the North Atlantic and Europe (Ayarzagüena et al., 2018; Joshi et al., 2021; Abid et al., 2021, 2023; Sabatani and Gualdi, 2025), and also regarding the potential role of the PDO as a modulating mechanism (Fernández-Castillo et al., 2025). In particular, the study by Sabatani and Gualdi (2025) highlighted that model biases in the North Pacific jet stream and in the southeast Asia wave source in historical runs from CMIP6 models contribute to the differences in the ENSO-EAP teleconnection across the different models. Similarly, O'Reilly (2025) found that North Pacific jet biases also contribute to this teleconnection's differences across state-of-the-art seasonal forecasting systems. Here, using a conceptually different approach in which we analyse how the teleconnection changes across different time periods within a single model, the signals obtained are fairly similar, pointing to a consistent mechanism by which changes in the Indian Ocean convection and North Pacific climatological jet stream affect the strength of the ENSO-EAP teleconnection, favouring a strong teleconnection in some periods while a weak ENSO-EAP teleconnection in other epochs.

Even though the long piControl simulations have enabled us to overcome the issue of too small sample sizes (and the associated high uncertainty in the signals), they also present certain limitations. It is important to acknowledge that the necessary simplification or parametrisation of some of the physical processes in climate models inevitably leads to model-specific biases, for instance in the jet stream, which have a notable impact on the simulated ENSO teleconnection patterns (Sabatani and Gualdi, 2025). This fact could be observed in Figure 1, which illustrates the significant

underestimation of the teleconnection strength in the models analysed, and the range of teleconnection patterns across the different models. Therefore, it cannot be ruled out that part of the separation between the POSCORR and WEAKCORR samples may be explained by noise. As a result of these uncertainties, aggregating models in a multi-model mean often results in a weak signal. This circumstance was clearly visible in the analysis of mechanisms, where the signals were often weak and occasionally not robust in terms of cross-model agreement. Nevertheless, most of the signals from individual models were sufficiently strong to be clearly distinguished from sampling variability. Hence, while observations and reanalyses are constrained by limited sample sizes that hinder statistical significance and robustness, in climate models the uncertainty or lack or robustness mainly stems from the aggregation of models with distinct biases. Regardless of this limitation, the approach employed here remains highly advantageous and does contribute to a better understanding of the processes involved, proving to be a suitable tool in order to formulate stronger hypotheses. In this sense, the results from this study underscore the pertinence of performing targeted sensitivity experiments. In these, the possible modulating role of the different pathways or the low-frequency modes of variability can be studied more thoroughly. Moreover, while our study focused on the broad, seasonal-scale mechanisms contributing to the multidecadal variability, we underscore the pertinence of analysing the mechanisms at the synoptic and subseasonal scales by studying the dynamics of the storm track and eddy-driven jet, the propagation of eddy energy from the North Pacific into the North Atlantic as well as changes in blocking frequency, as these are important to understand how the seasonal-mean circulation anomalies in response to ENSO shape up in the North Atlantic (O'Reilly et al., 2024). These analyses are a subject of ongoing work involving the mentioned sensitivity experiments.

In summary, despite their intrinsic limitations, observational and now also model-based studies so far reinforce the hypothesis of a meaningful non-stationarity of the ENSO-EAP teleconnection, with different potential drivers such as the PDO which still need to be addressed with sensitivity experiments. The different approaches to study the non-stationarity offer necessary complementary insights that, altogether, allow us to build a comprehensive understanding of the teleconnection, its stationarity and its underlying mechanisms. Ultimately, this can result in a better understanding of seasonal variability and predictability in the North Atlantic and European region.

Acknowledgements

This research work was funded by the Ministry for the Ecological Transition and the Demographic Challenge (MITECO) and the European Commission NextGenerationEU (Regulation EU 2020/2094), through CSIC's Interdisciplinary Thematic Platform Clima (PTI-Clima), and was supported by the Spanish national project PID2024-158995NB-I00. This work used supercomputing resources of the German Climate Computing Centre (Deutsches Klimarechen-zentrum, DKRZ) under project ID 1153. The work of PFC at the Meteorology Department of the University of Reading was supported by CSIC's movility program iMove (IMOVE25210).

Data availability statement

The model data that support the findings of this study are openly available in the Earth System Grid Federation (ESGF) portal (https://esgf-node.ornl.gov/). ERA5 data are openly available from the Copernicus Climate Change Service Climate Data Store (https://cds.climate.copernicus.eu/datasets).

Conflict of interest

The authors declare no competing interests.

References

Abid, M. A., Kucharski, F., Molteni, F. and Almazroui, M. (2023) Predictability of indian ocean precipitation and its north atlantic teleconnections during early winter. *Npj Climate and Atmospheric Science*, **6**, 17.

Abid, M. A., Kucharski, F., Molteni, F., Kang, I.-S., Tompkins, A. M. and Almazroui, M. (2021) Separating the indian and pacific ocean impacts on the euro-atlantic response to enso and its transition from early to late winter. *Journal of Climate*, **34**, 1531–1548.

Ayarzagüena, B., Ineson, S., Dunstone, N. J., Baldwin, M. P. and Scaife, A. A. (2018) Intraseasonal effects of el niño–southern oscillation on north atlantic climate. *Journal of Climate*, **31**, 8861–8873.

Boucher, O., Servonnat, J., Albright, A. L., Aumont, O., Balkanski, Y., Bastrikov, V., Bekki, S., Bonnet, R., Bony, S., Bopp, L. et al. (2020) Presentation and evaluation of the ipsl-cm6a-lr climate model. *Journal of Advances in Modeling Earth Systems*, **12**, e2019MS002010.

Brands, S. (2017) Which enso teleconnections are robust to internal atmospheric variability? *Geophysical Research Letters*, **44**, 1483–1493.

Brönnimann, S. (2007) Impact of el niño–southern oscillation on european climate. *Reviews of Geophysics*, **45**.

Danabasoglu, G., Lamarque, J.-F., Bacmeister, J., Bailey, D., DuVivier, A., Edwards, J., Emmons, L., Fasullo, J., Garcia, R., Gettelman, A. et al. (2020) The community earth system model version 2 (cesm2). *Journal of Advances in Modeling Earth Systems*, **12**, e2019MS001916.

Deser, C., Simpson, I. R., Phillips, A. S. and McKinnon, K. A. (2018) How well do we know enso's climate impacts over north america, and how do we evaluate models accordingly? *Journal of Climate*, **31**, 4991–5014.

Eyring, V., Bony, S., Meehl, G. A., Senior, C. A., Stevens, B., Stouffer, R. J. and Taylor, K. E. (2016) Overview of the coupled model intercomparison project phase 6 (cmip6) experimental design and organization. *Geoscientific Model Development*, **9**, 1937–1958.

Fan, L., Liu, Q., Wang, C. and Guo, F. (2017) Indian ocean dipole modes associated with different types of enso development. *Journal of Climate*, **30**, 2233–2249.

Fernández-Castillo, P., Losada, T., Rodríguez-Fonseca, B., García-Maroto, D., Mohino, E. and Durán, L. (2025) Multidecadal variability of the enso early-winter teleconnection to europe and implications for seasonal forecasting. *npj Climate and Atmospheric Science*, **8**, 272.

Geng, X., Zhao, J. and Kug, J.-S. (2023) Enso-driven abrupt phase shift in north atlantic oscillation in early january. *Npj Climate and Atmospheric Science*, **6**, 80.

Gill, A. E. (1980) Some simple solutions for heat-induced tropical circulation. *Quarterly Journal of the Royal Meteorological Society*, **106**, 447–462.

Graf, H.-F. and Zanchettin, D. (2012) Central pacific el niño, the "subtropical bridge," and eurasian climate. *Journal of Geophysical Research: Atmospheres*, **117**.

Gutjahr, O., Putrasahan, D., Lohmann, K., Jungclaus, J. H., von Storch, J.-S., Brüggemann, N., Haak, H. and Stössel, A. (2019) Max planck institute earth system model (mpi-esm1. 2) for the high-resolution model intercomparison project (highresmip). *Geoscientific Model Development*, **12**, 3241–3281.

Hardiman, S., Dunstone, N., Scaife, A., Smith, D., Ineson, S., Lim, J. and Fereday, D. (2019) The impact of strong el niño and la niña events on the north atlantic. *Geophysical Research Letters*, **46**, 2874–2883.

Harnik, N., Seager, R., Naik, N., Cane, M. and Ting, M. (2010) The role of linear wave refraction in the transient eddy–mean flow response to tropical pacific sst anomalies. *Quarterly Journal of the Royal Meteorological Society*, **136**, 2132–2146.

Hersbach, H., Bell, B., Berrisford, P., Hirahara, S., Horányi, A., Muñoz-Sabater, J., Nicolas, J., Peubey, C., Radu, R., Schepers, D. et al. (2020) The era5 global reanalysis. *Quarterly journal of the royal meteorological society*, **146**, 1999–2049.

Hoskins, B. J. and Karoly, D. J. (1981) The steady linear response of a spherical atmosphere to thermal and orographic forcing. *Journal of Atmospheric Sciences*, **38**, 1179–1196.

Hou, J., Fang, Z. and Geng, X. (2023) Recent strengthening of the enso influence on the early winter east atlantic pattern. *Atmosphere*, **14**, 1809.

Jiménez-Esteve, B. and Domeisen, D. I. (2018) The tropospheric pathway of the enso–north atlantic teleconnection. *Journal of Climate*, **31**, 4563–4584.

Joshi, M. K., Abid, M. A. and Kucharski, F. (2021) The role of an indian ocean heating dipole in the enso teleconnection to the north atlantic european region in early winter during the twentieth century in reanalysis and cmip5 simulations. *Journal of Climate*, **34**, 1047–1060.

Kelley, M., Schmidt, G. A., Nazarenko, L. S., Bauer, S. E., Ruedy, R., Russell, G. L., Ackerman, A. S., Aleinov, I., Bauer, M., Bleck, R. et al. (2020) Giss-e2. 1: Configurations and climatology. *Journal of Advances in Modeling Earth Systems*, **12**, e2019MS002025.

Kiladis, G. N. and Diaz, H. F. (1989) Global climatic anomalies associated with extremes in the southern oscillation. *Journal of climate*, **2**, 1069–1090.

King, M. P., Herceg-Bulić, I., Bladé, I., García-Serrano, J., Keenlyside, N., Kucharski, F., Li, C. and Sobolowski, S. (2018) Importance of late fall enso teleconnection in the euro-atlantic sector. *Bulletin of the American Meteorological Society*, **99**, 1337–1343.

Li, L., Yu, Y., Tang, Y., Lin, P., Xie, J., Song, M., Dong, L., Zhou, T., Liu, L., Wang, L. et al. (2020) The flexible global ocean-atmosphere-land system model grid-point version 3 (fgoals-g3): Description and evaluation. *Journal of Advances in Modeling Earth Systems*, **12**, e2019MS002012.

Li, Y. and Lau, N.-C. (2012) Impact of enso on the atmospheric variability over the north atlantic in late winter—role of transient eddies. *Journal of Climate*, **25**, 320–342.

Mariotti, A., Zeng, N. and Lau, K.-M. (2002) Euro-mediterranean rainfall and enso—a seasonally varying relationship. *Geophysical research letters*, **29**, 59–1.

Mathieu, P., Sutton, R., Dong, B. and Collins, M. (2004) Predictability of winter climate over the north atlantic european region during enso events. *Journal of Climate*, **17**, 1953–1974.

McKenna, M. and Karamperidou, C. (2023) The impacts of el niño diversity on northern hemisphere atmospheric blocking. *Geophysical Research Letters*, **50**, e2023GL104284.

Molteni, F. and Brookshaw, A. (2023) Early-and late-winter enso teleconnections to the euro-atlantic region in state-of-the-art seasonal forecasting systems. *Climate Dynamics*, **61**, 2673–2692.

Molteni, F., Roberts, C. D., Senan, R., Keeley, S. P., Bellucci, A., Corti, S., Fuentes Franco, R., Haarsma, R., Levine, X., Putrasahan, D. et al. (2020) Boreal-winter teleconnections with tropical indo-pacific rainfall in highresmip historical simulations from the primavera project. *Climate Dynamics*, **55**, 1843–1873.

O'Reilly, C. H. (2025) Signal-to-noise errors in early winter euro-atlantic predictions linked to weak enso teleconnections and pervasive jet biases. *Quarterly Journal of the Royal Meteorological Society*, **151**, e4952.

O'Reilly, C. H., Drouard, M., Ayarzagüena, B., Ambaum, M. H. and Methven, J. (2024) The role of storm-track dynamics in the intraseasonal variability of the winter enso teleconnection to the north atlantic. *Quarterly Journal of the Royal Meteorological Society*, **150**, 2069–2086.

Park, S., Shin, J., Kim, S., Oh, E. and Kim, Y. (2019) Global climate simulated by the seoul national university atmosphere model version 0 with a unified convection scheme (sam0-unicon). *Journal of Climate*, **32**, 2917–2949.

Raganato, A., Abid, M. A. and Kucharski, F. (2025) The combined link of the indian ocean dipole and enso with the north atlantic–european circulation during early boreal winter in reanalysis and the ecmwf seas5 hindcast. *Journal of Climate*, **38**, 445–460.

Rieke, O., Greatbatch, R. J. and Gollan, G. (2021) Nonstationarity of the link between the tropics and the summer east atlantic pattern. *Atmospheric Science Letters*, **22**, e1026.

Righi, M., Andela, B., Eyring, V., Lauer, A., Predoi, V., Schlund, M., Vegas-Regidor, J., Bock, L., Brötz, B., de Mora, L. et al. (2020) Earth system model evaluation tool (esmvaltool) v2. 0–technical overview. *Geoscientific Model Development*, **13**, 1179–1199.

Rodríguez-Fonseca, B., Suárez-Moreno, R., Ayarzagüena, B., López-Parages, J., Gómara, I., Villamayor, J., Mohino, E., Losada, T. and Castaño-Tierno, A. (2016) A review of enso influence on the north atlantic. a non-stationary signal. *Atmosphere*, **7**, 87.

Ropelewski, C. F. and Halpert, M. S. (1987) Global and regional scale precipitation patterns associated with the el niño/southern oscillation. *Monthly weather review*, **115**, 1606–1626.

Sabatani, D. and Gualdi, S. (2025) Enso teleconnections with the nae sector during december in cmip5/cmip6 models: impacts of the atmospheric mean state. *npj Climate and Atmospheric Science*, **8**, 226.

Sardeshmukh, P. D. and Hoskins, B. J. (1988) The generation of global rotational flow by steady idealized tropical divergence. *Journal of Atmospheric Sciences*, **45**, 1228–1251.

Swart, N. C., Cole, J. N., Kharin, V. V., Lazare, M., Scinocca, J. F., Gillett, N. P., Anstey, J., Arora, V., Christian, J. R., Hanna, S. et al. (2019) The canadian earth system model version 5 (canesm5. 0.3). *Geoscientific Model Development*, **12**, 4823–4873.

Takaya, K. and Nakamura, H. (2001) A formulation of a phase-independent wave-activity flux for stationary and migratory quasigeostrophic eddies on a zonally varying basic flow. *Journal of the Atmospheric Sciences*, **58**, 608–627.

Tatebe, H., Ogura, T., Nitta, T., Komuro, Y., Ogochi, K., Takemura, T., Sudo, K., Sekiguchi, M., Abe, M., Saito, F. et al. (2019) Description and basic evaluation of simulated mean state, internal variability, and climate sensitivity in miroc6. *Geoscientific Model Development*, **12**, 2727–2765.

Toniazzo, T. and Scaife, A. A. (2006) The influence of enso on winter north atlantic climate. *Geophysical Research Letters*, **33**.

Volodin, E., Mortikov, E., Kostrykin, S., Galin, V. Y., Lykossov, V., Gritsun, A., Diansky, N., Gusev, A. and Iakovlev, N. (2017) Simulation of the present-day climate with the climate model inmcm5. *Climate dynamics*, **49**, 3715–3734.

Yukimoto, S., Kawai, H., Koshiro, T., Oshima, N., Yoshida, K., Urakawa, S., Tsujino, H., Deushi, M., Tanaka, T., Hosaka, M. et al. (2019) The meteorological research institute earth system model version 2.0, mri-esm2. 0: Description and basic evaluation of the physical component. *Journal of the Meteorological Society of Japan. Ser. II*, **97**, 931–965.

Zhang, W., Wang, Y., Jin, F.-F., Stuecker, M. F. and Turner, A. G. (2015) Impact of different el niño types on the el niño/iod relationship. *Geophysical Research Letters*, **42**, 8570–8576.

Supplementary Files

This is a list of supplementary files associated with this preprint. Click to download.

- SupplementarymaterialENSOCMIP6v2.01.pdf